DIMENSIONAL ERRORS IN SELECTIVE LASER MELTING PRODUCTS RELATED TO DIFFERENT ORIENTATIONS AND PROCESSING PARAMETERS

DIMENZIJSKE NAPAKE NA IZDELKIH, IZDELANIH S SELEKTIVNIM LASERSKIM TALJENJEM, GLEDE NA RAZLIČNE ORIENTACIJE IN PROCESNE PARAMETRE

Snehashis Pal[1*], Vanja Kokol[1], Nenad Gubeljak[1], Miodrag Hadzistevic[2], Radovan Hudak[3], Igor Drstvensek[1]

[1]University of Maribor, Faculty of Mechanical Engineering, Smetanova ulica 17, 2000 Maribor, Slovenia
[2]University of Novi Sad, Faculty of Technical Sciences, Trg Dositeja Obradovica 6, Novi Sad 106314, Serbia
[3]Technical University of Kosice, Department of Biomedical Engineering and Measurement, Letna 9, 042 00 Kosice, Slovakia

This research has investigated the changes of dimensions with changes of the Energy Density (ED), processing parameters and build up direction wise of Ti-6Al-4V alloy products manufactured by the Selective Laser Melting (SLM) process. The selected processing parameters were laser power, scanning speed, and hatch spacing in several combinations, keeping the layer thickness constant during all three steps of the studies. Four orientations have been considered for a specimen to build up in different directions for each of the selected combinations of processing parameters. The SLM process is characterized by the high laser energy inputs into a metallic powder layer in a short interaction time that occurs several thermal related issues that significantly affect the shape and dimensions of the part. The results show that ED, as well as its processing parameters, have significant influences on the product's dimensions. The building orientation has a great impact on the dimensional accuracy.

Keywords: dimensional error, processing parameters, building orientation, selective laser melting

Avtorji opisujejo raziskavo dimenzijskih sprememb zaradi sprememb energijske gostote (ED), procesnih parametrov in smeri nanašanja posameznih plasti nastajajočega izdelka, izdelovanega s postopkom selektivnega laserskega taljenja (SLM). Avtorji so izbrali naslednje procesne parametre: moč laserja, hitrost skeniranja in velikost dozirne odprtine v treh različnih kombinacijah. Pri tem je ostala debelina posamezne plasti konstantna pri vseh treh raziskovanih primerih. Raziskovali so vpliv štirih različnih orientacij pri vsaki od izbranih procesnih kombinacij. Za SLM proces je značilno, da velik prenos energije laserja na plast kovinskega prahu v zelo kratkem času interakcije povzroči več termično povezanih učinkov, ki močno vplivajo na obliko in dimenzije izdelka. Rezultati raziskave so pokazali, da ED kakor tudi procesni parametri močno vplivajo na dimenzije izdelka. Smer izgradnje izdelka ima tudi velik vpliv na dimenzijsko točnost.

Ključne besede: dimenzijske napake, procesni parametri, orientacija gradnje izdelka, selektivno lasersko taljenje

1 INTRODUCTION

Selective Laser Melting (SLM) is a tens-of-micrometers-thick layer-wise material addition technique that allows the fabricating of complex three-dimensional products.[1] This technology directly transfers a virtual Computer-Aided Designed (CAD) model into a metallic part.[2,3] High flexibility including low manufacturing costs and timing attract manufacturers to fabricate molds, automobile parts, aerospace parts and customized orthopedic implants of complex shape.[4] The production process consists of the highly localized fusing of metal particles, during which many thermodynamic and physical phenomena occur in a very short time.[5] The temperature of the action area rises suddenly and creates a small melt pool, which in turn cools down rapidly, solidifies and undergoes several phase changes. This process induces expansion and shrinkage during the manufacturing of each track and layer, respectively.[6] During melting at a certain local place, the tiny melt pool also being affected by the same mechanism.[7]

Since the thermal effect is induced by the energy input, depending on laser power, time of scanning and re-melting volume, the processing parameters included in Energy Density (ED) should have a high impact on the thermal behavior of the melt pool as well as the entire layer, including the preceding layers.[8] The processing parameters are the laser power, scanning speed, hatch spacing, and layer thickness. Prior to sending the CAD file to the SLM machine, it has to be sliced into micron-sized layers (typically 25 μm).[9] The parts are then built up layer-wise in the vertical direction. Accordingly, the powder re-coater deposits the powder particles layer by layer and the laser melts the powder in the form of cross-section of each layer between the two consecutive re-coatings. The areas of the cross-sections of a CAD part differ, which leads to different scanning times.[10] Thus, the thermal effect would vary on the

*Corresponding author's e-mail:
snehashiseu@gmail.com

product segment due to a different orientation or built up direction. Eventually, the dimensions of a product would be altered due to different thermal effects in its different building direction.

In the SLM fabrication process, different types of dimensional inaccuracies remain in the products, which lowers the repeatability rate and the overall achievable accuracy of the SLM process. Previous research also showed that the geometrical complexity and orientation in the work space significantly influences the achievable accuracy and productivity of the additive manufacturing (AM) machines.[11,12] Since the expansion and shrinkage of the parts are influenced by the processing parameters, the presented study has explored the dimensional accuracy and errors occurring in specimens built by different processing parameters and building orientations. The considered dimensions in this study were length, width and height/thickness of the specimens.

The Ti-6Al-4V alloy is a lightweight metal with a low thermal conductivity and a high mechanical strength, corrosion resistance and biocompatibility.[13] These make the Ti-6Al-4V alloy the most appropriate metal for biomedical applications as well as for automobile and aerospace industries, and therefore one of the most common materials in SLM fabrication.[14–16] For that reason it has been chosen for the presented study.

2 EXPERIMENTAL PART

2.1 Material

The used material was fully dense, Ti-6Al-4V, extra low interstitial alloy powder with a granulation of 5–40 μm provided by Dentaurum, Germany. The built tray was made of the Ti-6Al-4V alloy to avoid any uneven heat conduction.

2.2 Experimental set-up

The study was focused on the dimensional changes with respect to the building directions and the processing parameters included in the ED. The ED is proportional to the laser power and inversely proportional to the scanning speed, the hatch spacing between two parallel consecutive scanning tracks, i.e., the laser beam central distance between two consecutive scanning tracks, and the layer thickness to be fused. The volumetric ED can be defined by Equation (1).[4,17]

$$ED = \frac{P}{v \cdot h \cdot H} \qquad (1)$$

where P is the laser power, v is the scanning speed, h is the hatch spacing, and H is the layer thickness.

To find the optimum values of the three processing parameters, three steps of the studies were performed. The first step focused on scanning speeds in the range of 150 mm/s to 1000 mm/s in seven different sets by keeping the other parameters constant, which assign seven isolated EDs in the range of 39 J/mm^3 to 260 J/mm^3, as listed in **Table 1**. Four subsets of specimens having different orientations were selected in each set of the first step. The second step was based on five different laser powers in the range of 55 W to 95 W, combined with five different scanning speeds, keeping ED and other parameters constant, which are listed in **Table 2**. The optimum ED, as well as the optimal range of scanning speeds, were selected based on the previous step considering several metallurgical properties. Similarly, four subsets having different orientations were laid out in each set of the second step. The third step focused on hatch spacing by changing the track overlapping from 10 % to 55 %, as listed in **Table 3**. The scanning speeds and other parameters were kept in the optimal range obtained from the previous steps. Only the longitudinal-vertical orientation of the specimen was considered in the third step based on positive results of the previous steps. The sliced layer thickness was 25 μm throughout the entire experiment.

The samples were fabricated in a protected environment filled with argon with 0.8 % of remaining oxygen, at 20 °C in a mLab Cusing machine, made by Concept Laser, Lichtenfels, Germany. The machine uses 100W Yb:fiber laser (YLM 100 AC – IPG Photonics, Burbach, Germany), working in a continuous-wave mode with a 1070±10 nm wavelength. The diameter of the focus point was 0.11 mm, focused by a f-theta lens with a focal distance of 163 mm. The laser emits in TEM$_{00}$ and has the beam mode quality factor M^2 1.09. All the samples were built upon a 2 mm high support structure, except the gauge portion of the widthwise built up specimens where the support height was 4 mm, according to the requirement.

Table 1: List of the processing parameters having different scanning speeds and EDs to fabricate the samples in the first step

Sample Set number	Laser power (W)	Scanning speed (mm/s)	Track overlapping (%)	Hatch spacing (mm)	Layer thickness (mm)	Energy Density (J/mm^3)
I-1	75	1000	30	0.077	0.025	39
I-2	75	800	30	0.077	0.025	49
I-3	75	600	30	0.077	0.025	65
I-4	75	400	30	0.077	0.025	97
I-5	75	300	30	0.077	0.025	130
I-6	75	200	30	0.077	0.025	195
I-7	75	150	30	0.077	0.025	260

Table 2: List of the processing parameters having different laser powers and scanning speeds to fabricate the samples in the second step

Sample Set number	Laser power (W)	Scanning speed (mm/s)	Track overlapping (%)	Hatch spacing (mm)	Layer thickness (mm)	Energy Density (J/mm^3)
II-1	95	760	30	0.077	0.025	65
II-2	85	680	30	0.077	0.025	65
II-3	75	600	30	0.077	0.025	65
II-4	65	520	30	0.077	0.025	65
II-5	55	440	30	0.077	0.025	65

Table 3: List of the processing parameters having different hatch spacings and scanning speeds to fabricate the samples in the third step

Sample Set number	Laser power (W)	Scanning speed (mm/s)	Track overlapping (%)	Hatch spacing (mm)	Layer thickness (mm)	Energy Density (J/mm³)
III-1	65	405	10	0.099	0.025	65
III-2	65	430	15	0.0935	0.025	65
III-3	65	455	20	0.088	0.025	65
III-4	65	485	25	0.0825	0.025	65
III-5	65	520	30	0.077	0.025	65
III-6	65	560	35	0.0715	0.025	65
III-7	65	605	40	0.066	0.025	65
III-8	65	660	45	0.0605	0.025	65
III-9	65	725	50	0.055	0.025	65
III-10	65	805	55	0.0495	0.025	65

The dimensions were measured from the cuboid samples as well as tensile specimens. The nominal measurements of the cuboid samples were 8 mm × 8 mm × 8 mm. The height (Z direction) and side (X and Y direction) dimensions were measured as built from the cubic samples fabricated with several combinations of processing parameters. The tensile specimens were measured over their overall length, gauge width, and thickness. They were fabricated in four different orientations as well as with several combinations of processing parameters. The selected orientations were lengthwise inclined (subset-1), lengthwise vertical (subset-2), widthwise inclined (subset-3), widthwise vertical (subset-4) as shown in **Figure 1a-d**. The inclination angle was 30° from the vertical plane for each inclined specimen. The CAD model dimensions of the tensile specimen were 33 mm overall length, 2 mm gauge width and 1 mm thick, as shown in **Figure 1e**. The sides of the cuboid samples and tensile specimens were parallel to the horizontal plane, i.e., parallel to the X-axis or Y-axis. Th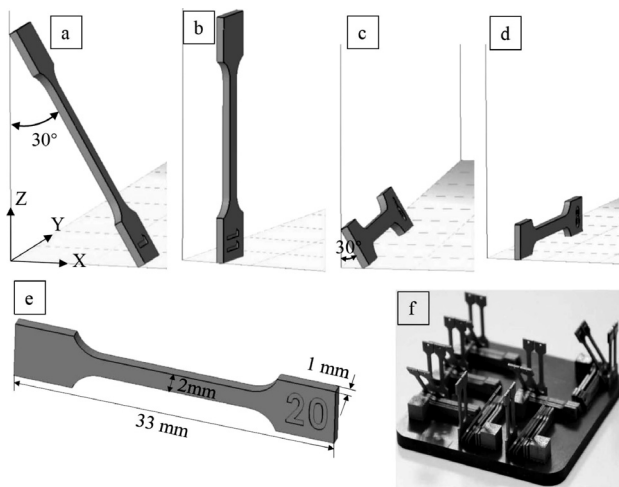e base of the cuboid samples was parallel to the XY plane, and the height corresponds to the Z axis, which is the build-up direction. Scanning directions were interchanged between 45° and 135° along the X-axis for each consecutive layer. Therefore, there was no influence of the scanning direction on the side-wise lengths of the samples. The dimensions of the as-built samples were measured using a Mitutoyo digital Vernier caliper at room temperature and without any post-processing. The absolute error of the measurements was 0.099 mm.

3 RESULTS AND DISCUSSION

The measurement discrepancies were observed for most of the specimens. The dimensions changed with the changing of the processing parameters. Significant dimensional changes were observed in the differently oriented specimens as well. The reasons for the inaccuracy of the specimens are described in detail in the continuation.

3.1 Cuboid samples dimensions

Figure 2a shows the side and height dimensional errors of the cuboid samples manufactured in different EDs at the first step of the studies. As the scanning of consecutive layers was made in the perpendicular direction, the side-wise dimensions in the X direction or Y direction of a cubic sample are almost equal and below the absolute error of the measurement. Therefore, only the lengths of the sides instead of the X and Y measurements of the samples are listed among the results. There is a significant difference between the dimensions of the side and the height in all the sets of the samples. The heights are bigger than their sides, except for the sample in set-I-7, manufactured with a very high
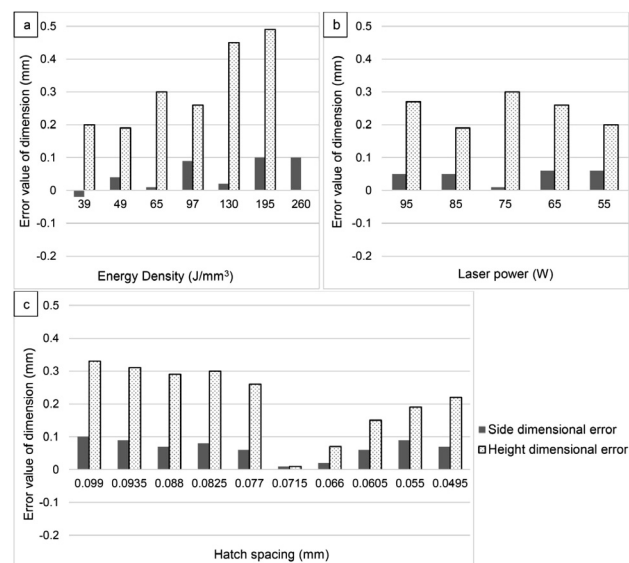

Figure 1: Specimens for different orientations, where: a) subset-1 is lengthwise inclined, b) subset-2 is lengthwise vertical, c) subset-3 is widthwise inclined, d) subset-4 is widthwise vertical, e) dimensions in CAD model, and f) a photograph of the samples as manufactured in the first step.

Figure 2: Dimensional error of the cuboid samples manufactured with different: a) EDs (and scanning speeds), b) laser powers, c) hatch spacing

ED (260 J/mm³). Among the sets, both dimensions, side, and height, slightly increase with a rise of the ED. The best side measurement was obtained in cuboid set-I-3 manufactured with 65 J/mm³ ED and 600 mm/s scanning speed. The cuboid set-II-1 has the smallest side error and the height error is not much different from the lowest height error.

By combining the cuboid samples from set-I-1 to set-I-6 into three groups containing two consecutive samples (set-I-1 and set-I-2 belong to group-1, set-I-3 and set-I-4 belong to group-2 and so on), it can be observed that each group has similar results. The odd numbered sample has a bit lower side-length error than the following even-numbered sample in each group and the heights are also almost equal in both samples in each group. This is due to the ED values and the scanning speeds (influencing cooling rates) lying in the same effective range in each group. The melt-pool volume occupies the tiny space in the actioning layer and a smaller space in the preceding layer.[8] Except for the last preceding layer, the other preceding layers stay at a lower temperature because of the low thermal conductivity of the Ti-6Al-4V alloy.[1,5] The area of the scanned layer slightly expands during the action. The increase of the ED causes an increase of the temperature at the scanning area that causes a higher melt pool volume as well as the higher expansion of material that reduces the crystallinity.[18] The reduction of the crystallinity leads to a reduction in the shrinkage. On the other hand, a higher scanning speed causes a higher cooling rate, which leads to lack of crystallinity time. Therefore, an even sample shrinks less than the following odd sample.

Shrinkage is not identical along the Z and X or Y directions since the product builds up along the Z direction and the scanning works along the X or Y direction alternately. The side is affected by the area of the layer to be scanned, whereas its height is affected by the layer thickness. Therefore, it has been observed that the expansion is significantly higher in the built up (Z) directions compared to the X and Y directions. As the set-I-7 was manufactured with an extremely low scanning speed and high ED, it had sufficient time for crystallization, which leads to a high shrinkage in the Z direction and expansion in the X and Y directions. Additionally, at the highest ED, a huge spattering of material was observed that caused a reduction of material, which led to the lowering of the height.[19,20] During scanning of the starting layer on the support structure, the first layer melt-pool volume depends on ED, and the higher ED caused a higher melt-pool volume,[19] which occupied the area below the expected bottom surface of the product. Therefore, rising the ED from 39 J/mm³ to 195 J/mm³ caused higher additional dimensions from the set-I-1 to set-I-2, respectively.

A quite similar dimensional error effect can be observed in the cuboid samples in the second step as in the first step, which is illustrated in **Figure 2b**. Almost similar dimensional errors were observed in all the sets due to the same ED employed in all the sets. As the employed energy and cooling rate provoke the expansion and shrinkage of the material; therefore, the laser power does not have any significant correlation with them.

Figure 2c illustrates the dimensional error of the cuboid samples manufactured in the third step considering different hatch spacing. The results show that the samples manufactured with a smaller track overlapping (higher hatch spacing) shrunk less because of the shorter scanning time for the entire layer. Thus, the first few samples cool down faster, which caused lower crystallinity. Increasing the track overlapping (shorter hatch spacing) leads to an increase of the scanning time and reduces the cooling rate. A lower cooling rate allows more time for the molecules to arrange in an order, which rises the crystallinity, which in turn causes higher shrinkage. As a result, the specimens in set-III-6 (manufactured with 35 % track overlapping and 560 mm/s scanning speed) shrink optimally and come closer to the dimensions of the CAD file after cooling. A further increase of the track overlapping happens along with the higher scanning speed, which again reduces the scanning time and raises the cooling rate. Additionally, higher track overlapping causes a higher temperature at the overlapping area, which causes a bigger melt-pool volume at the starting layer. Thus, the dimensions increase from the cuboid set-III-7 onwards.

3.1 Tensile specimens' dimensions fabricated in different directions

The dimensional variations and phenomena of the cuboid samples are reflected in the tensile specimens manufactured in different orientations. The lengthwise inclined and vertically built up specimens exhibit a longer length compared to the widthwise inclined and vertical specimens in all sets of the first step of the study, built up in different EDs. Interestingly, **Figure 3** shows that the lengths of the lengthwise build up specimens (subset-1 and subset-2) for each set are higher than the CAD dimensions and the lengths of the widthwise build up specimens (subset-3 and subset-4) for each set are lower than the CAD dimensions. Similar variations were observed in cuboid samples where the heights (in the Z direction) are longer than the side (in X or Y direction). Most of the lengthwise build up specimens have a length of about 33.25±0.10 mm from set-I-1 to set-I-5, where higher EDs performed higher length up to 33.49 mm, where the original CAD length was 33 mm. On the other hand, widthwise built up specimens shrunk below their original lengths to about 32.92±0.08 mm. Comparing the horizontal lengths of both the cuboid samples and the tensile specimens (considering lengthwise only), it can be seen that a bigger (longer) scanning area produces a higher shrinkage than a smaller (shorter) area, which corresponds to the phenomenon of thermal expansion and is somewhat expected.
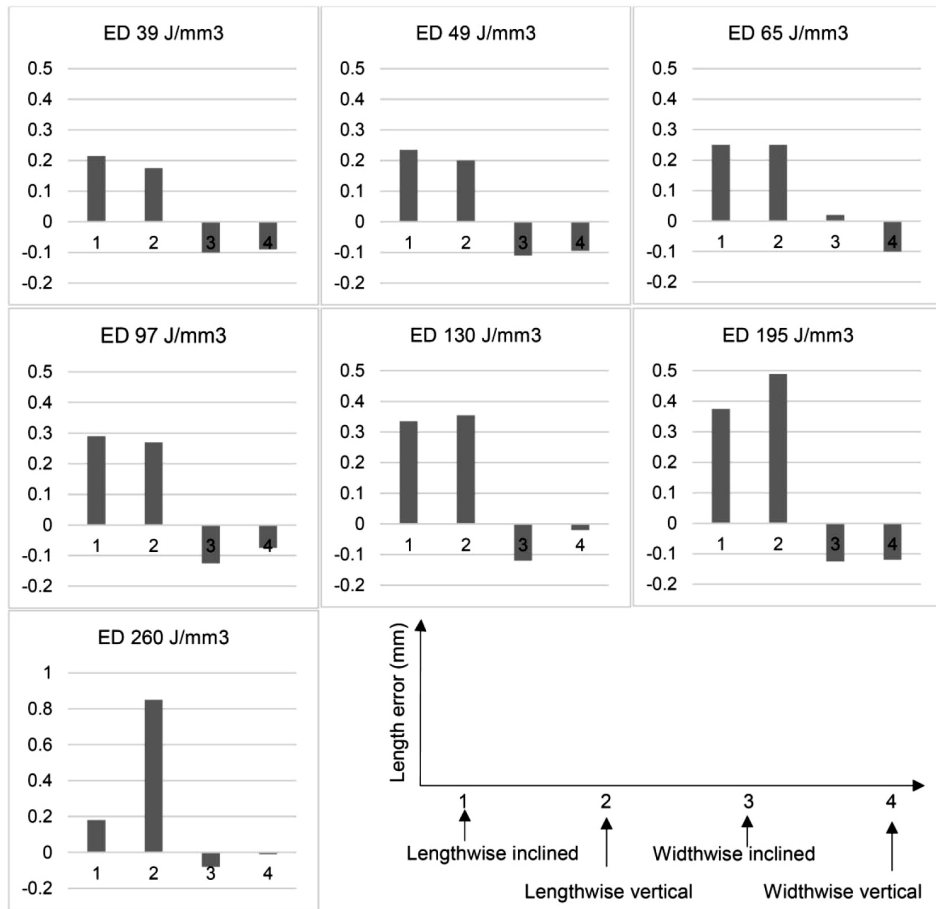
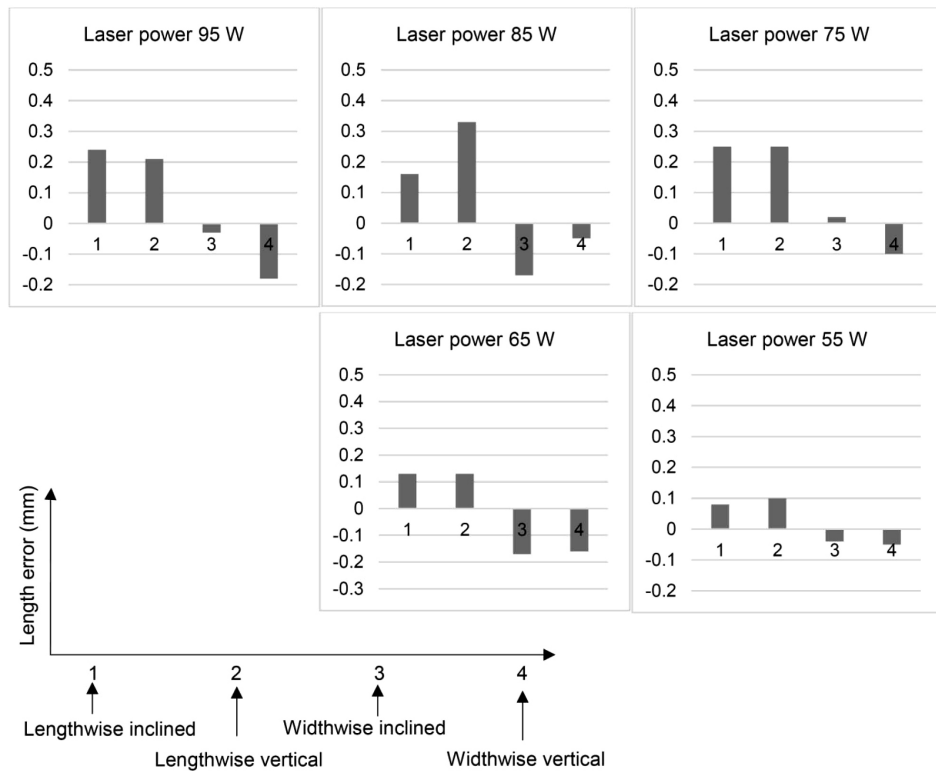**Figure 3:** Lengthwise dimensional error of the specimens fabricated in different orientations for every different ED

Figure 4: Lengthwise dimensional error of the specimens fabricated in different orientations and with different laser power
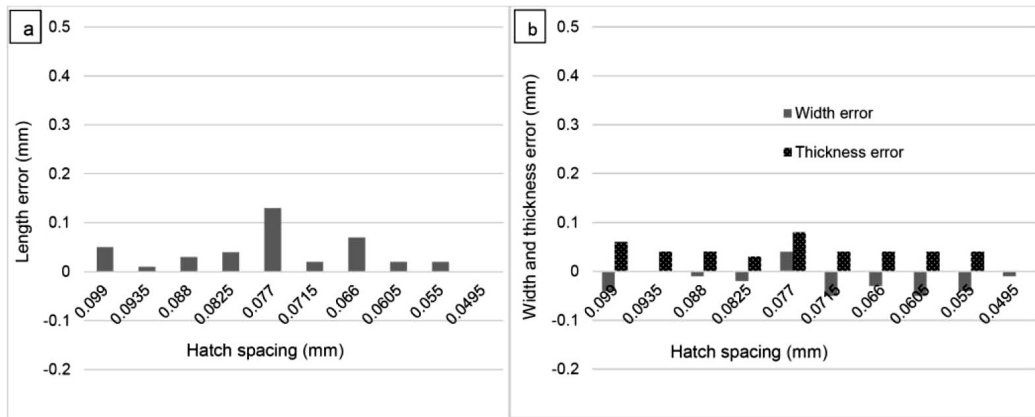
Figure 5: Dimensional errors of the tensile specimens built up in lengthwise vertical with different hatch spacing, where: a) shows the length errors and b) shows width and thickness errors

The same effect was observed in the second step of the experiment. **Figure 4** demonstrates that the lengthwise built up specimens (subset-1 and subset-2) have a longer length than the widthwise built up specimens (subset-3 and subset-4). As previously, the lengthwise built up specimens are longer and inversely, the widthwise built up specimens are shorter than the nominal length.

Figure 5a shows the dimensional errors of the tensile specimens built up lengthwise vertical with different hatch spacing. The specimen built up with the highest track overlapping of 55 % and scanning speed of 805 mm/s, has an accurate dimension of 33 mm. Though the specimen has high track overlapping, the scanning speed was also high as well as the scanning area per layer being very small, which is 2 mm × 1 mm. Therefore, the layers got sufficient time for crystallizing
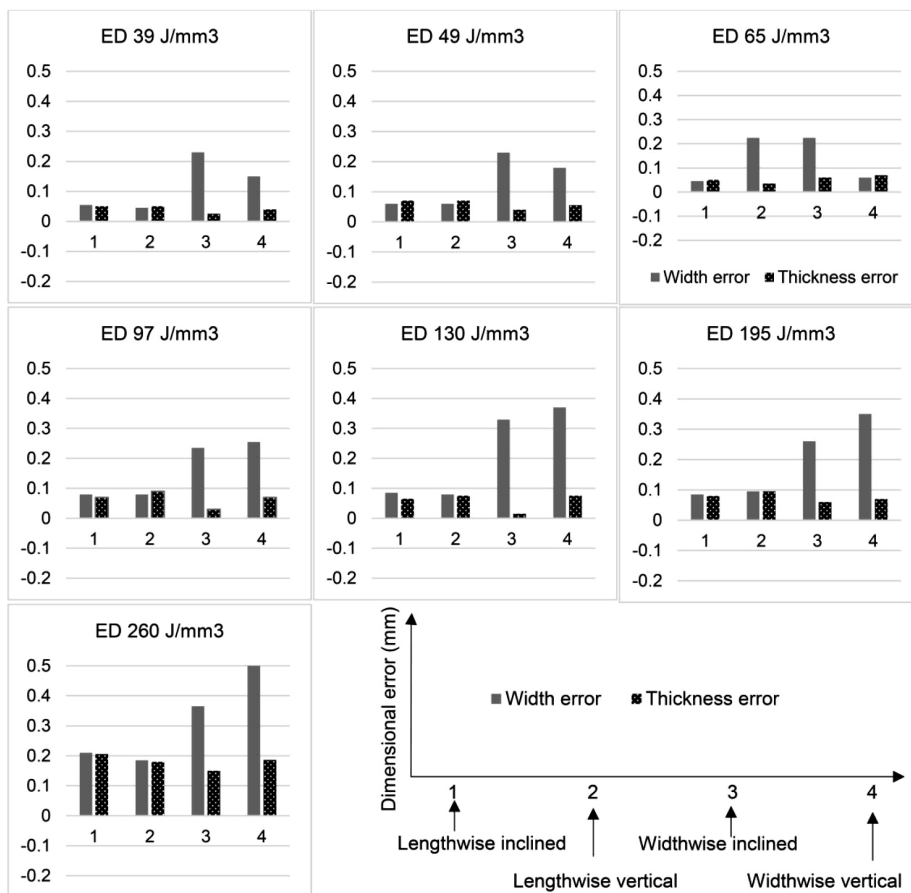

Figure 6: Width and thickness error of the specimens manufactured in different orientations with different EDs
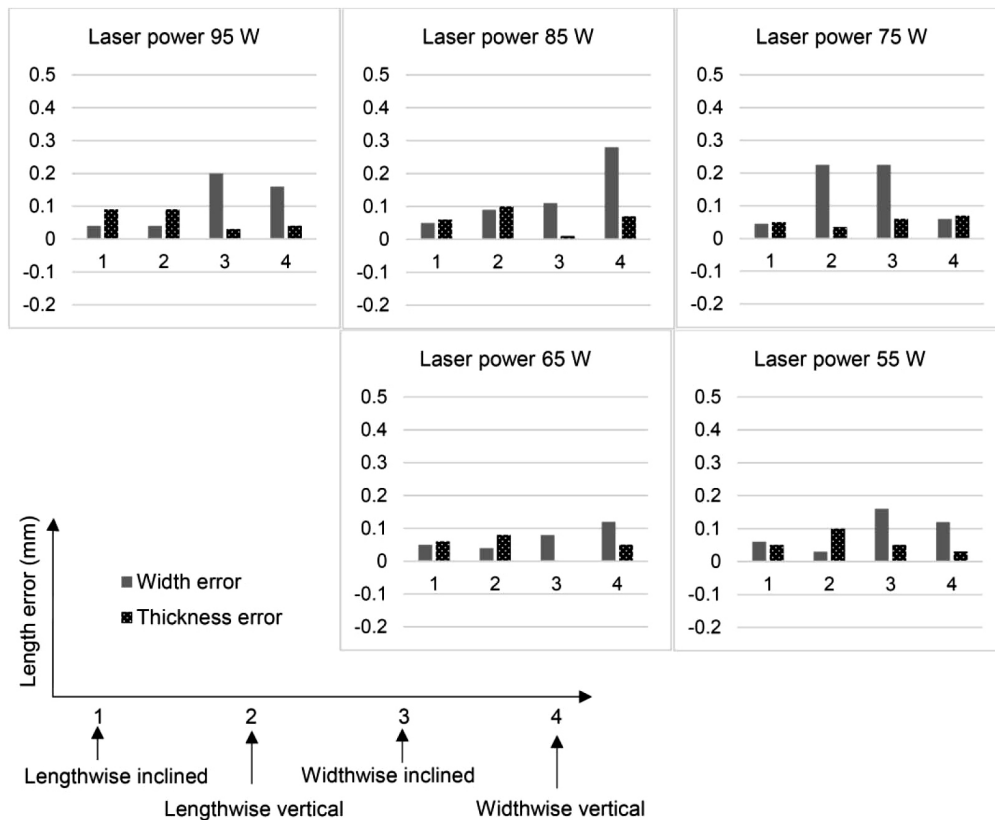
Figure 7: Width and thickness error of the specimens manufactured in different orientations with different laser powers

and shrinking to achieve the desired size in the Z direction.

The previous dimensional consequences show that the Z direction has a higher dimension than the X and Y directions. The width of a specimen is perpendicular to its length, which means the specimens oriented in the Z direction have the width in the Y direction and the specimens oriented in Y direction have their widths in the Z direction. **Figure 6** shows that the results are similar to the previous results, which means the Z length is longer than the Y length. Hence, the widths of the specimens subset-3 and subset-4 have a higher value than the specimens in subset-1 and subset-2 in the first step.

Certainly, **Figure 7** proves that widths of the specimens built up in different orientations in the second set have similar dimensions. Subset-3 and Subset-4 have higher widths than subset-1 and subset-2.

From **Figure 5b** it is clear that the tensile specimen number 10 in the third step has the desired dimensions with the lowest hatch spacing (0.0495 mm), i.e., the highest track overlapping (55 %). Therefore, slightly different results are observed between the cuboid samples and the tensile specimens. The optimally dimensioned cube was produced in the set-III-6, whereas the optimum dimensioned tensile specimen was manufactured lengthwise vertically in the set-III-10.

4 CONCLUSIONS

This study has reported the changes and errors in the dimensions of Ti-6Al-4V alloy products fabricated with different EDs, scanning speeds, laser powers, hatch spacings, and building orientations. The majority of the results show that the length in the Z direction is higher than the X or Y direction as well as the errors are mostly positive in the Z directions, whereas they are negative in the X and Y directions. The dimensions are significantly influenced by the input energy and the cooling rate during fusion and amalgamation. These thermodynamic and physical mechanisms directly depend on the ED and the scanning speed. The laser power has no influence if the ED remains constant. Eventually, the desired dimension was achieved in the cuboid sample set-III-6. The tensile specimen built up lengthwise vertical in set-III-10 showed the desired dimensions as in the CAD model.

Acknowledgements

6 REFERENCES

[1] J. Yang, H. Yang, H. Yu, Z. Wang, H. Wang, X. Zeng, A novel approach to in-situ fabricate Ti-6Al-4V alloy with graded microstructure and property by selective laser melting, Mater Lett., 215 (**2018**), 246-249, doi:10.1016/j.matlet.2017.12.098

[2] M. Vaezi, H. Seitz, S. Yang, A review on 3D micro-additive manufacturing technologies, Int J Adv Manuf Technol., 67 (**2013**) 5–8, 1721–1754, doi:10.1007/s00170-012-4605-2

[3] S. A. Adekanye, R. M. Mahamood, E. T. Akinlabi, M. G.Owolabi, Additive manufacturing: the future of manufacturing, Mater Tehnol., 51 (**2017**) 5, 709–715, doi:10.17222/mit.2016.261

[4] L. Thijs, F. Verhaeghe, T. Craeghs, J. V. Humbeeck, J. P. Kruth. A study of the microstructural evolution during selective laser melting of Ti-6Al-4V, Acta Mater., 58 (**2010**) (9), 3303–3312, doi:10.1016/j.actamat.2010.02.004

[5] H. Shipley, D. McDonnell, M. Culleton, R. Coull, R. Lupoi, G. O'Donnell, D. Trimble, Optimisation of process parameters to address fundamental challenges during selective laser melting of Ti-6Al-4V: A review, Int J Mach Tools Manuf., 128 (**2018**) 1–20, doi:10.1016/j.ijmachtools.2018.01.003

[6] S. Barui, S. Chatterjee, S. Mandal, A. Kumar, B. Basu, Microstructure and compression properties of 3D powder printed Ti-6Al-4V scaffolds with designed porosity: Experimental and computational analysis, Mater Sci Eng C, 70 (**2017**), 812–823, doi:10.1016/j.msec.2016.09.040

[7] J. Song, W. Wu, L. Zhang, B. He, L. Lu, X. Ni, Q. Long, G. Zhu, Role of scanning strategy on residual stress distribution in Ti-6Al-4V alloy prepared by selective laser melting, Optik (Stuttg), 170 (**2018**), 342–352, doi:10.1016/j.ijleo.2018.05.128

[8] M. Masoomi, S. M. Thompson, N. Shamsaei, Laser powder bed fusion of Ti-6Al-4V parts: Thermal modeling and mechanical implications, Int J Mach Tools Manuf, 118-119 (**2017**) 73–90, doi:10.1016/j.ijmachtools.2017.04.007

[9] S. Pal, I. Drstvensek, Physical behaviors of materials in selective laser melting process, DAAAM Int Sci B., Vienna 2018, 239–256, doi:10.2507/daaam.scibook.2018.21

[10] H. Yu, J. Yang, J. Yin, Z. Wang, X. Zeng, Comparison on mechanical anisotropies of selective laser melted Ti-6Al-4V alloy and 304 stainless steel, Mater Sci Eng A, 695 (**2017**) 92–100, doi:10.1016/j.msea.2017.04.031

[11] U. Kostevsek, T. Brajlih, J. Balic, Ž. Kadivnik, I. Drstvensek, Development of productivity estimation model for mass-customized production by selective laser melting, Rapid Prototyp J, 24 (**2018**) 3, 670–676, doi:10.1108/RPJ-06-2017-0120

[12] T. Brajlih, B. Valentan, J. Balic, I. Drstvensek, Speed and accuracy evaluation of additive manufacturing machines, Rapid Prototyp J, 17 (**2011**) 1, 64–75, doi:10.1108/13552541111098644

[13] S. Y. Chen, J. C. Huang, C. T. Pan, C. H. Lin, T. L. Yang, Y. S. Huang, C. H. Ou, L. Y. Chen, D. Y. Lin, H. K. Lin, T. H. Li, J. S. C. Jang, C. C. Yang, Microstructure and mechanical properties of open-cell porous Ti-6Al-4V fabricated by selective laser melting, J Alloys Compd., 713 (**2017**), 248–254, doi:10.1016/j.jallcom.2017.04.190

[14] R. Wauthle, J. Van Der Stok, S. A. Yavari, J. V. Humbeeck, J. P. Kruth, A. A. Zadpoor, H. Weinans, M. Mulier, J. Schrooten, Additively manufactured porous tantalum implants, Acta Biomater., 14 (**2015**), 217–225, doi:10.1016/j.actbio.2014.12.003

[15] N. T. Aboulkhair, I. Maskery, C. Tuck, I. Ashcroft, N. M. Everitt, On the formation of AlSi10Mg single tracks and layers in selective laser melting: Microstructure and nano-mechanical properties, J Mater Process Technol., 230 (**2016**), 88–98, doi:10.1016/j.jmatprotec.2015.11.016

[16] B. Nie, H. Huang, S. Bai, J. Liu, Femtosecond laser melting and resolidifying of high-temperature powder materials, Appl Phys A Mater Sci Process, 118 (**2014**) 1, 37–41, doi:10.1007/s00339-014-8897-y

[17] S. Pal, H. R. Tiyyagura, I. Drstvenšek, C. S. Kumar, The effect of post-processing and machining process parameters on properties of stainless steel PH1 product produced by direct metal laser sintering, Procedia Eng., 149 (**2016**), 359–365, doi:10.1016/j.proeng.2016.06.679.

[18] T. H. C. Childs, A. E. Tontowi, Selective laser sintering of a crystalline and a glass-filled crystalline polymer: Experiments and simulations, Proc Inst Mech Eng, Part B: J Eng Manuf., 215 (**2001**) 11, 1481–1495, doi:10.1243/0954405011519330

[19] S. Pal, G. Lojen, V. Kokol, I. Drstvensek, Evolution of metallurgical properties of Ti-6Al-4V alloy fabricated in different energy densities in the Selective Laser Melting technique, J Manuf Process., 35 (**2018**), 538–546, doi:10.1016/j.jmapro.2018.09.012

[20] S. Pal, N. Gubeljak, R. Hudak, G. Lojen, V. Rajtukova, J. Predan, V. Kokol, I. Drstvensek, Tensile properties of selective laser melting products affected by building orientation and energy density, Mater Sci Eng A, 743 (**2018**), 637–647, doi:10.1016/J.MSEA.2018.11.130